RESEARCH ARTICLE OPEN ACCESS

Cerebrospinal Fluid-In Gradient of Cortical and Deep Gray Matter Damage in Multiple Sclerosis

Martina Rubin, MD, Elisabetta Pagani, MSc, Paolo Preziosa, MD, PhD, Alessandro Meani, MSc, Loredana Storelli, PhD, Monica Margoni, MD, PhD, Massimo Filippi, MD, and Maria A. Rocca, MD

Correspondence
Dr. Rocca
rocca.mara@hsr.it

Neurol Neuroimmunol Neuroinflamm 2024;11:e200271. doi:10.1212/NXI.0000000000200271

Abstract

Background and Objectives

A CSF-in gradient in cortical and thalamic gray matter (GM) damage has been found in multiple sclerosis (MS). We concomitantly explored the patterns of cortical, thalamic, and caudate microstructural abnormalities at progressive distances from CSF using a multiparametric MRI approach.

Methods

For this cross-sectional study, from 3T 3D T1-weighted scans, we sampled cortical layers at 25%-50%-75% depths from pial surface and thalamic and caudate bands at 2-3-4 voxels from the ventricular-GM interface. Using linear mixed models, we tested between-group comparisons of magnetization transfer ratio (MTR) and R2* layer-specific z-scores, CSF-in across-layer z-score changes, and their correlations with clinical (disease duration and disability) and structural (focal lesions, brain, and choroid plexus volume) MRI measures.

Results

We enrolled 52 patients with MS (33 relapsing-remitting [RRMS], 19 progressive [PMS], mean age: 46.4 years, median disease duration: 15.1 years, median: EDSS 2.0) and 70 controls (mean age 41.5 ± 12.8). Compared with controls, RRMS showed lower MTR values in the outer and middle cortical layers (false-discovery rate [FDR]-$p \leq 0.025$) and lower R2* values in all 3 cortical layers (FDR-$p \leq 0.016$). PMS had lower MTR values in the outer and middle cortical (FDR-$p \leq 0.016$) and thalamic (FDR-$p \leq 0.048$) layers, and in the outer caudate layer (FDR-$p = 0.024$). They showed lower R2* values in the outer cortical layer (FDR-$p = 0.003$) and in the outer thalamic layer (FDR-$p = 0.046$) and higher R2* values in all 3 caudate layers (FDR-$p \leq 0.031$). Both RRMS and PMS had a gradient of damage, with lower values closer to the CSF, for cortical (FDR-$p \leq 0.002$) and thalamic (FDR-$p \leq 0.042$) MTR. PMS showed a gradient of damage for cortical R2* (FDR-$p = 0.005$), thalamic R2* (FDR-$p = 0.004$), and caudate MTR (FDR-$p \leq 0.013$). Lower MTR and R2* of outer cortical, thalamic, and caudate layers and steeper gradient of damage toward the CSF were significantly associated with older age, higher T2-hyperintense white matter lesion volume, higher thalamic lesion volume, and lower brain volume ($\beta \geq 0.08$, all FDR-$p \leq 0.040$). Lower MTR of outer caudate layer was associated with more severe disability ($\beta = -0.26$, FDR-$p = 0.040$). No correlations with choroid plexus volume were found.

Discussion

CSF-in damage gradients are heterogeneous among different GM regions and through MS course, possibly reflecting different dynamics of demyelination and iron loss/accumulation.

From the Neuroimaging Research Unit (M.R., E.P., P.P., A.M., L.S., M.M., M.F., M.A.R.), Division of Neuroscience; Neurology Unit (M.R., P.P., M.M., M.F., M.A.R.), IRCCS San Raffaele Scientific Institute; Vita-Salute San Raffaele University (M.R., P.P., M.F., M.A.R.); Neurorehabilitation Unit (M.M., M.F.); and Neurophysiology Service (M.F.), IRCCS San Raffaele Scientific Institute, Milan, Italy.

Go to Neurology.org/NN for full disclosures. Funding information is provided at the end of the article.

The Article Processing Charge was funded by the authors.

Glossary

CP = choroid plexus; **DIR** = double-inversion recovery; **EDSS** = Expanded Disability Status Scale; **FDR** = false-discovery rate; **FLAIR** = fluid attenuation inversion recovery; **GM** = gray matter; **HC** = healthy controls; **MS** = multiple sclerosis; **MTR** = magnetization transfer ratio; **PMS** = progressive multiple sclerosis; **RRMS** = relapsing-remitting multiple sclerosis; **SWI** = susceptibility-weighted image; **WM** = white matter.

Introduction

The accumulation of focal white matter (WM) lesions resulting from blood-brain barrier disruption and immune cell infiltration stands as the primary pathologic feature of multiple sclerosis (MS). However, recent pathologic studies have identified a CSF-in gradient of damage,[1] being more severe at periventricular[2,3] and subpial levels, and potentially related to the infiltration of proinflammatory cytokines from the CSF. This pathologic process may contribute not only to WM and gray matter (GM) lesion accrual but also to microstructural damage accumulation in thalamic[2] and cortical[4] normal-appearing tissue.

The application of advanced high-field (3T) or ultra-high-field (7T) MRI techniques specific to different MS-related pathologic processes has further supported the relevance of surface-in damage gradient in both CSF-adjacent GM[5-10] and WM.[10-12] In thalamic and cortical GM, a gradient of microstructural alterations, in diffusivity abnormalities, lower magnetization transfer ratio (MTR),[9] lower T1/T2-weighted ratio,[8] and increased T2*[5-7] has been observed from the earliest phases of the disease,[6,8,9] becoming more severe in progressive patients with MS.[5,6,9]

To comprehensively characterize CSF-mediated pathology in patients with MS and its accumulation across different phases of the disease, we conducted a multiparametric MRI study. Our investigation may leverage to better understand the heterogeneous pathologic processes affecting cortex and deep GM structures in MS because they are close to CSF but have different cytoarchitectural properties, thus being differently susceptible to inflammatory insults.

To this aim, we evaluated concomitantly cortical and thalamic CSF-in gradients of damage through MTR and R2* trends in MS disease phases. We also analyzed the caudate, another CSF-adjacent GM nucleus,[13-18] known to be involved in different neurodegenerative conditions,[19] which may provide novel insights into CSF-driven inflammatory injury. The combined evaluation of MTR and R2* allows a more specific distinction between different pathologic substrates of damage because MTR provides information on myelin density, whereas R2* is specific for iron content and, to a lesser extent, for myelin.[20-23] To explore possible common driving mechanisms, we correlated CSF-in damage gradient with T2-hyperintense WM and GM lesion volume and atrophy measures. In addition, given increasing evidence of choroid plexus (CP) enlargement as a marker of chronic inflammation,[24-26] we also investigated the correlation between CP volume and CSF-in damage trends, to define possible relations between proinflammatory environment and CP remodelling observed in MS.[24-26] Finally, we addressed the clinical relevance of gradient abnormalities through their correlation with clinical variables (disease duration and Expanded Disability Status Scale [EDSS] score).

Methods

Standard Protocol Approvals, Registrations, and Patient Consents

Approval was received from the institutional ethical standards committee on human experimentation of IRCCS Ospedale San Raffaele for any experiments using human participants (Protocol No. 2015–33). Written informed consent was obtained from all participants before study participation according to the Declaration of Helsinki.

Study Population

From the database of Neuroimaging Research Unit, IRCCS San Raffaele Scientific Institute, we retrospectively selected 52 consecutive patients with MS (33 relapsing-remitting [RRMS] and 19 progressive [PMS]) who underwent the same MRI protocol between May 2017 and May 2022. Inclusion criteria were age 18 years or older, diagnosis of MS according to 2017 revision of the McDonald criteria, relapse-free and steroid-free status for at least 1 month before study entry, absence of other neurologic or psychiatric conditions, and a stable treatment for MS for at least 6 months.

We also selected 70 consecutive healthy controls (HC) with no neurologic diseases or systemic disorders potentially affecting the CNS, with a completely normal neurologic examination.

Clinical Assessment

Within 3 days from MRI acquisition, all patients with MS underwent a complete neurologic examination, with EDSS score rating, definition of clinical phenotype, and recording of disease-modifying treatments, performed by a neurologist blinded to MRI findings.

MRI Data Acquisition

To be included, the following brain MRI sequences were required to have been acquired for each patient with MS and HC using a 3.0 T Philips Ingenia CX scanner (receiving Coil =

dS-Head-32): (1) sagittal three-dimensional (3D) fluid attenuation inversion recovery (FLAIR), (2) sagittal 3D T1-weighted turbo field echo, (3) sagittal 3D double-inversion recovery (DIR), (4) 3D fast field echo with and without an off-resonance radiofrequency saturation pulse, and (5) 3D susceptibility-weighted image (SWI), both magnitude and phase images for each echo were saved. Details of the MRI protocol are available in the eMethods.

Quantification of Lesions and Atrophy

Focal T2-hyperintense WM lesions were identified by a fully automated and validated approach using 3D FLAIR and 3D T1-weighted as input images.[27] T2-hyperintense WM lesion volume was obtained for each patient from their lesion masks, after visual check of the results of automatic segmentations.

On DIR images, after exclusion of possible artifacts,[28] cortical lesions were identified following published recommendations.[28] Both cortical lesions confined to the cortical ribbon without involving the underlying subcortical WM (pure intracortical) and mixed WM/GM lesions (leukocortical) with a predominant (>50%) extension in the cortex were considered. Manual detection of cortical lesions on DIR images was performed by consensus of 2 experienced raters (P.P. and M.R.). In case of disagreement, a third rater evaluated the lesions and reached a final decision (M.A.R.). Thereafter, cortical lesion volume was estimated using a local thresholding segmentation technique (Jim 8.0 software).

Thalamic and caudate lesions were defined as focal hyperintensities on DIR images that were also hypointense on 3D T1-weighted images and with a predominant (>50%) extension in the thalamus or caudate nuclei. Manual detection of thalamic and caudate lesions on DIR was performed by consensus of 2 experienced raters (P.P. and M.R), with evaluation of a third rater (M.A.R.) in case of disagreement, then, the lesion volume was estimated using a local thresholding segmentation technique (Jim 8.0 software).

The segmentation of whole brain, cortex, WM and CSF, and their normalized volumes were obtained from 3D T1-weighted images, after lesion-filling, using the FSL SIENAx software. Thalamic and caudate segmentations were derived using the FIRST tool, and their volume was normalized for head size using the SIENAx scaling factor.

Cortical Thickness Quantification

Cortical pial and WM surfaces were obtained using the FreeSurfer software (version 7.1.1), according to a multistep procedure that calculates the cortical-WM and CSF-WM (pial) boundary in the 3D T1-weighted space (Figure 1).[29] Topologic defects in cortical surfaces due to WM and leukocortical lesions were avoided applying lesion filling before the processing and manually corrected, if necessary. Mean cortical thickness was measured in each subject computing the distance (mm) between cortical-WM border and pial surface.[29]

Creation of Thalamic and Caudate Bands

Using a pipeline implemented in Matlab (R2012b, MathWorks), concentric bands from the ventricular CSF were generated within the thalamus: a dilation of one voxel was applied on the CSF mask to obtain the intersection between the thalamus and the dilated CSF masks; this intersection was the seed region to calculate the geodesic distance of each

Figure 1 Methodologic Process to Obtain Cortical, Thalamic, and Caudate Layers at Progressive Distance From the CSF

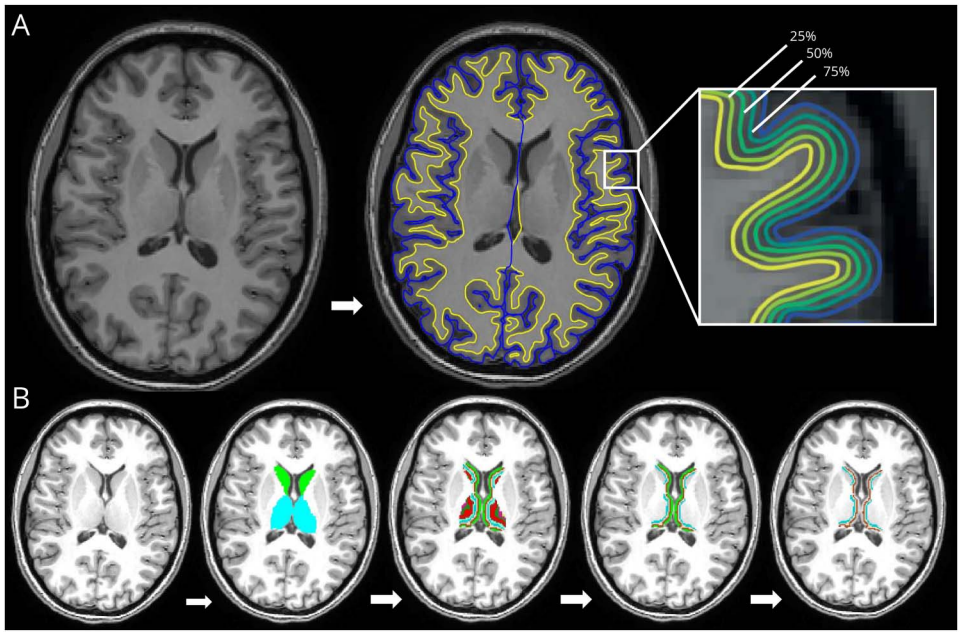

(A) From left to right, subsequent steps to obtain 3 approximately equidistant cortical layers: original 3D T1-weighted sequence; pial and GM-WM boundary surface segmentations obtained with FreeSurfer software; surfaces at 25%, 50%, and 75% of the cortical thickness from the GM-WM boundary surface (image for illustrative purpose, as long as the surfaces were obtained in 3 dimensions). (B) From left to right, subsequent steps to obtain 3 thalamic and caudate 1 voxel-thick layers: original 3D T1-weighted sequence; thalamic and caudate segmentations obtained with the FSL SIENAx software (FIRST tool); concentric bands generated from the ventricular CSF using a pipeline implemented in Matlab which calculates the geodesic distance of each voxel from the CSF, in the 3 dimensions; extraction of the first 4 layers from the GM-CSF interface; subtraction of the first layer adjacent to the CSF. See text for further details. GM = gray matter; WM = white matter.

thalamic voxel from CSF, in the 3 dimensions.[8] The same process was applied on caudate (head and body) (Figure 1).

MTR and R2* Analysis at Progressive Distances From CSF

MTR images were calculated according to the formula: MTR = (M0[non saturated] − MS[saturated]/M0 × 100). R2* maps were obtained by fitting multiecho SWI with a method based on Auto-Regression on Linear Operations.[30]

Each individual MTR and R2* map was coregistered to 3D T1-weighted image and to the corresponding cortical surface without reslicing by using a boundary-based registration algorithm.[7,31] MTR and R2* values were then sampled along the surfaces at 25% (outer layer), 50% (middle layer), and 75% (inner layer) of the cortical thickness from pial to cortical-WM interface. To this aim, surfaces at 25%, 50%, and 75% of the cortical thickness were calculated from the cortical-WM boundary surface and averaged over the entire cortex (Figure 1).

After coregistration of each individual MTR and R2* map to 3D T1-weighted image, MTR and R2* were sampled in each band of the thalamus and caudate at a progressive distance of 1-2-3-4 voxels from the ventricular surface. As previously done,[8,11,12,32] for both deep GM structures, the first layer adjacent to the CSF was excluded to limit partial volume confounding effects (Figure 1). As proinflammatory cytokine infiltration, microglial reactivity and neuroaxonal damage have been observed up to 10 mm from the thalamus-CSF boundary in progressive patients with MS,[2] we expected to find a gradient of damage in all the layers investigated. For consistency between the 3 GM structures evaluated, the second layer (closer to CSF) was defined as 'outer layer', whereas the fourth layer (farther from CSF) as 'inner layer'.

Choroid Plexus Volume Quantification

The CPs of the lateral ventricles were manually segmented on 3D T1-weighted sequences using a local thresholding segmentation technique (Jim 8.0 software), and their volume was calculated.[25] Reliability of the method, in interrater and intrarater agreement, has already been shown in a previous study.[33] The CPs of the third and fourth ventricles were not included, given their inconstant visualization. The lateral ventricles were obtained by summing their relevant parts from FreeSurfer segmentation. Volumes of CPs and lateral ventricles were normalized for head size using the SIENAx scaling factor.

Statistical Analysis

Demographic and clinical variables were compared between groups using χ^2, Fisher exact and Mann-Whitney *U* tests, or linear models, as appropriate.

Age-adjusted and sex-adjusted linear models were performed to assess differences in MRI features between HC and patients with MS, as well as between clinical phenotypes. Lesion volumes were square-root-transformed. Normalized brain and lateral ventricle volumes were included as additional covariates in the analysis of normalized CP volume.[25]

To estimate MTR and R2* expected lifespan trajectories in the 3 evaluated layers of cortex, thalamus, and caudate nucleus, we fitted linear mixed models, accounting for nested design (layers within participants), to HC data, considering sex, age, and the layer as predictors. The inclusion of age squared and higher-order interaction terms was evaluated according to the Akaike information criterion. For each structure, we investigated the occurrence of a physiologic gradient of MTR or R2* values across layers in the CSF-in direction and quantified it assessing mean CSF-in MTR and R2* changes per layer.

Estimated parameters from the described models were then used to convert MTR and R2* ratio values measured in patients with MS to z-scores, which represent a standardized measure of deviation from the sex-specific, age-specific, and layer-specific expected values in the control population. We assessed and compared MTR and R2* layer-specific z-scores in patients with MS, as a whole and according to clinical phenotype, with linear mixed models, testing the null hypothesis that mean z-scores equal zero (i.e., healthy population expected value). Mean CSF-in z-score changes per layer were also evaluated to investigate the presence of a gradient of microstructural abnormalities across layers in the CSF-in direction.

Correlations between MTR and R2* layer-specific z-scores and CSF-in z-score changes per layer in the 3 structures in the whole MS group and in the 2 MS phenotypes were evaluated through Pearson correlation.

We finally explored the association of MTR and R2* layer-specific z-scores and CSF-in z-score changes per layer with demographic, clinical, and MRI (brain lesion and volumetric measures) variables, in patients with MS also according to clinical phenotypes, by linear mixed models.

Benjamini-Hochberg false-discovery rate (FDR) correction was performed to account for the overall number of tests performed, for each analysis separately. SAS release V.9.4 (SAS Institute, Cary, NC) was used for computations. p values < 0.05 were deemed statistically significant.

Data Availability

The corresponding author, who had complete access to all the data of the study, assumes responsibility for the integrity of the data and accuracy in the analysis. The anonymized data set used and analyzed for this study can be obtained from the corresponding author on reasonable request.

Results

Demographic, Clinical, and Conventional MRI Findings

Compared with HC, all MS, as well as both RRMS and PMS groups separately, had significantly higher T2-hyperintense WM lesion volume (FDR-p < 0.001), lower normalized volumes of the brain and thalamus (FDR-$p \leq 0.008$), and higher normalized volumes of CP (FDR-$p \leq 0.028$) and lateral

ventricles (FDR-$p \leq 0.002$). Compared with HC, whole MS and PMS groups were also significantly older ($p \leq 0.042$) and showed significantly lower normalized caudate volume (FDR-$p \leq 0.049$) and lower cortical thickness (FDR-$p \leq 0.017$). Compared with RRMS, PMS had significantly higher EDSS score ($p < 0.001$), higher T2-hyperintense WM, thalamic and cortical lesion volumes (FDR-$p \leq 0.028$), lower normalized brain, thalamic and cortical volumes (FDR-$p \leq 0.033$), lower cortical thickness (FDR-$p = 0.017$), and higher normalized lateral ventricle volume (FDR-$p = 0.017$) (Table 1).

MTR and R2* Values in Thalamic, Caudate Nucleus, and Cortical Layers in HC

Different age- and layer-effects of MTR and R2* patterns were observed in the 3 GM regions explored. With aging, thalamic MTR values showed a quadratic trend ($\beta = -0.001$; $p = 0.023$) with a peak around the age of 40 years in all the 3 layers explored. No significant changes in thalamic R2* values were observed through lifespan in any layer ($p \geq 0.149$). Caudate and cortical R2* values showed a linear increase with age for all layers (for the caudate nucleus: $\beta = 0.066$; $p < 0.001$; for the cortex: β-range = 0.026–0.035; all-p < 0.001). No significant changes in

Table 1 Main Demographic, Clinical, and Conventional MRI (Brain Lesion and Volumetric Measures) Variables of Healthy Controls and Patients With Multiple Sclerosis as a Whole and According to Their Disease Clinical Phenotype

			MS vs HC			RRMS vs HC	PMS vs HC	PMS vs RRMS
	HC (70)	MS (52)	*p* (FDR-*p*)	RRMS (33)	PMS (19)	*p* (FDR-*p*)	*p* (FDR-*p*)	*p* (FDR-*p*)
Mean age (SD) (range) [y]	41.5 (12.8) (20.2–64.5)	46.4 (9.7) (26.1–63.2)	0.025	45.5 (10.4) (26.1–63.2)	47.9 (8.3) (31.4–59.7)	0.129	0.042	0.377
Female/male (%)	40 (57)/30 (43)	29 (56)/23 (44)	0.880	18 (55)/15 (45)	11 (58)/8 (42)	0.804	0.953	0.815
Median DD (IQR) [y]	—	15.1 (6.0–23.0)	—	13.6 (4.0–22.3)	15.3 (7.0–23.0)	—	—	0.548
Median EDSS (IQR)	—	2.0 (1.0–5.5)	—	1.5 (1.0–1.5)	6.0 (4.5–6.5)	—	—	<0.001
DMT status (%): None/first line/ second line*	—	13 (25)/23 (44)/ 16 (31)	—	9 (27)/17 (52)/ 7 (21)	4 (21)/6 (32)/9 (47)	—	—	0.176
Median WM LV (IQR) [mL]	0.0 (0.0–0.3)	2.7 (1.0–7.1)	<0.001 (<0.001)	2.0 (0.8–4.0)	7.3 (2.8–16.0)	<0.001 (<0.001)	<0.001 (<0.001)	0.004 (0.008)
Median thalamic LV (IQR) [mL]	0.0 (0.0–0.0)	0.0 (0.0–0.1)	—	0.0 (0.0–0.0)	0.0 (0.0–0.1)	—	—	0.022 (0.028)
Median caudate LV (IQR) [mL]	0.0 (0.0–0.0)	0.0 (0.0–0.0)	—	0.0 (0.0–0.0)	0.0 (0.0–0.3)	—	—	0.283 (0.304)
Median cortical LV (IQR) [mL]	0.0 (0.0–0.0)	0.0 (0.0–0.1)	—	0.0 (0.0–0.1)	0.1 (0.0–0.2)	—	—	<0.001 (<0.001)
EM								
NBV (SE) [mL]	1,560 (4)	1,516 (7)	<0.001 (<0.001)	1,533 (8)	1,487 (11)	0.005 (0.008)	<0.001 (<0.001)	0.002 (0.003)
NTV (SE) [mL]	22.19 (0.14)	20.00 (0.28)	<0.001 (<0.001)	20.78 (0.28)	18.64 (0.43)	<0.001 (<0.001)	0.003 (<0.001)	<0.001 (0.001)
NCV (SE) [mL]	9.88 (0.11)	9.48 (0.15)	0.042 (0.049)	9.74 (0.16)	9.02 (0.27)	0.484 (0.484)	0.008 (0.012)	0.027 (0.033)
Cth (SE) [mm]	2.34 (0.01)	2.30 (1.17)	0.005 (0.008)	2.32 (0.01)	2.26 (0.02)	0.187 (0.208)	0.001 (0.002)	0.012 (0.017)
NCPV (SE) [mL]	2.58 (0.06)	2.95 (0.08)	0.001 (0.002)	2.90 (0.07)	3.03 (0.17)	0.002 (0.003)	0.022 (0.028)	0.451 (0.467)
NLVV (SE) [mL]	20.49 (1.17)	32.37 (2.08)	<0.001 (<0.001)	27.88 (1.74)	40.40 (4.29)	<0.001 (0.002)	<0.001 (0.001)	0.012 (0.017)

Abbreviations: Cth = cortical thickness; DD = disease duration; DMTs = disease modifying treatments; EDSS = Expanded Disability Status Scale; EM = estimated mean; FDR = false-discovery rate; HC = healthy controls; IQR = interquartile range; LV = lesion volume; NBV = normalized brain volume; NCPV = normalized choroid plexus volume; NCV = normalized caudate volume; NLVV = normalized lateral ventricle volume; NTV = normalized thalamic volume; PMS = progressive multiple sclerosis; RRMS = relapsing-remitting multiple sclerosis; SE = standard error; WM = white matter.
Comparisons performed by linear models (age), χ^2 (sex), Mann-Whitney U (disease duration and EDSS), and Fisher exact (DMTs status) tests. FDR-corrected (Benjamini-Hochberg procedure) results from age-adjusted and sex-adjusted linear models are reported for MRI features. Lesion volumes were square-root-transformed. Normalized brain and lateral ventricle volumes were included as additional covariates in the analysis of normalized choroid plexus volume.
First-line DMTs: interferon β-1a, dimethyl fumarate, teriflunomide, glatiramer acetate; 2nd line DMTs: natalizumab, fingolimod, siponimod, ocrelizumab, methotrexate.

Figure 2 Estimated Sex-Adjusted MTR and R2* Lifespan Trajectories in Cortical, Thalamic, and Caudate Layers of Healthy Controls

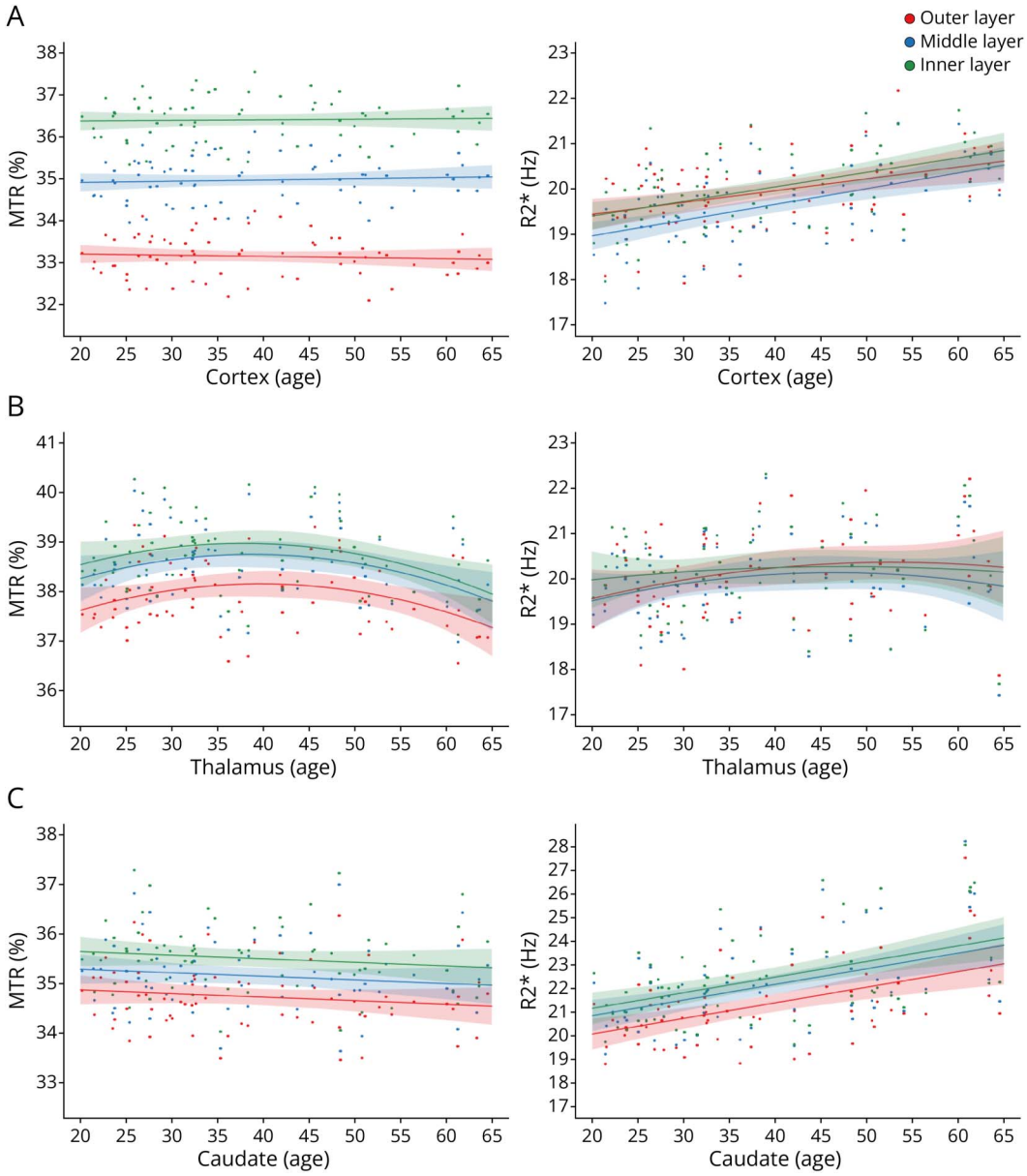

The figure shows in the first row MTR and R2* mean estimated sex-adjusted values (solid lines with 95% shaded CIs) in (A) cortex, (B) thalamus, and (C) caudate in outer, middle, and inner layers across ages in healthy controls (linear mixed model). See text for further details. CIs = confidence intervals; MTR = magnetization transfer ratio.

caudate or cortical MTR values were observed through lifespan in any layer (all $p > 0.269$) (Figure 2).

Regarding possible layer effects, MTR values showed a significant change per layer in the CSF-in direction in all 3 GM structures, with MTR values being significantly lower in the outer layer (for the thalamus, $\beta = 0.400$; $p < 0.001$; for the caudate, $\beta = 0.389$; $p < 0.001$; for the cortex, $\beta = 1.617$; $p < 0.001$). R2* values showed a significant change per layer in the CSF-in direction only in the caudate nucleus ($\beta = 0.540$, $p < 0.001$), with R2* values being significantly lower in the outer layer (Figure 2).

MTR and R2* Z-Scores in Cortical, Thalamic, and Caudate Layers in Patients With MS

In the cortex, compared with HC, patients with MS had significantly lower MTR in the outer (FDR-$p < 0.001$) and middle layers (FDR-$p = 0.019$), as well as significantly lower R2* in all the 3 layers explored (outer layer: FDR-$p < 0.001$; middle layer: FDR-$p = 0.004$; inner layer: FDR-$p = 0.014$). A significant CSF-in z-score change per layer (positive slope) of cortical MTR was found (FDR-$p < 0.001$), defining a more consistent cortical damage close to the CSF (Table 2, Figure 3).

Neurology: Neuroimmunology & Neuroinflammation (ISSN 2332-7812) is published by Wolters Kluwer Health, Inc. at 530 Walnut Street, Philadelphia, PA 19106-3621. Online ISSN: 2332-7812. Volume 11, Number 4, July 2024 e200271(7)

Table 2 Mean Estimated MTR and R2* Layer-Specific Z-Scores and CSF-In Z-Score Change per Layer in Patients With Multiple Sclerosis, as a Whole and According to Disease Phenotype, in Cortex, Thalamus, and Caudate

	Cortex													
	All MS				RRMS				PMS				PMS vs RRMS	
	EM (SE)	*p* (FDR-*p*)	ES (SE)	*p* (FDR-*p*)	EM (SE)	*p* (FDR-*p*)	ES (SE)	*p* (FDR-*p*)	EM (SE)	*p* (FDR-*p*)	ES (SE)	*p* (FDR-*p*)	*p* (FDR-*p*)	*p* (FDR-*p*)
MTR														
Outer	−0.95 (0.19)	<0.001 (<0.001)	0.34 (0.05)	<0.001 (<0.001)	−0.66 (0.24)	0.007 (0.025)	0.27 (0.06)	<0.001 (0.002)	−1.46 (0.31)	<0.001 (<0.001)	0.48 (0.09)	<0.001 (<0.001)	0.047 (0.098)	0.054 (0.108)
Middle	−0.46 (0.16)	0.004 (0.019)			−0.28 (0.19)	0.156 (0.226)			−0.78 (0.25)	0.003 (0.016)			0.117 (0.190)	
Inner	−0.27 (0.14)	0.053 (0.108)			−0.13 (0.17)	0.435 (0.503)			−0.50 (0.22)	0.028 (0.068)			0.191 (0.259)	
R2*														
Outer	−0.78 (0.15)	<0.001 (<0.001)	0.10 (0.04)	0.024 (0.061)	−0.67 (0.19)	0.001 (0.005)	0.02 (0.05)	0.765 (0.816)	−0.97 (0.24)	<0.001 (0.003)	0.25 (0.07)	0.001 (0.005)	0.340 (0.414)	0.009 (0.030)
Middle	−0.62 (0.17)	<0.001 (0.004)			−0.65 (0.21)	0.004 (0.016)			−0.58 (0.28)	0.039 (0.082)			0.854 (0.879)	
Inner	−0.58 (0.18)	0.003 (0.014)			−0.64 (0.23)	0.008 (0.027)			−0.47 (0.3)	0.124 (0.192)			0.650 (0.709)	
	Thalamus													
	MS				**RRMS**				**PMS**				**PMS vs RRMS**	
	EM (SE)	***p* (FDR-*p*)**	**ES (SE)**	***p* (FDR-*p*)**	**EM (SE)**	***p* (FDR-*p*)**	**ES (SE)**	***p* (FDR-*p*)**	**EM (SE)**	***p* (FDR-*p*)**	**ES (SE)**	***p* (FDR-*p*)**	***p* (FDR-*p*)**	***p* (FDR-*p*)**
MTR														
Outer	−0.57 (0.18)	0.003 (0.016)	0.17 (0.04)	<0.001 (0.002)	−0.36 (0.23)	0.118 (0.190)	0.12 (0.05)	0.015 (0.042)	−0.93 (0.30)	0.003 (0.016)	0.24 (0.06)	0.001 (0.005)	0.142 (0.209)	0.173 (0.245)
Middle	−0.35 (0.16)	0.038 (0.082)			−0.18 (0.20)	0.387 (0.456)			−0.65 (0.26)	0.017 (0.048)			0.171 (0.245)	
Inner	−0.24 (0.16)	0.138 (0.208)			−0.12 (0.20)	0.567 (0.640)			−0.46 (0.26)	0.090 (0.159)			0.308 (0.379)	
R2*														
Outer	−0.50 (0.20)	0.009 (0.030)	0.08 (0.04)	0.065 (0.124)	−0.38 (0.25)	0.136 (0.207)	−0.02 (0.05)	0.755 (0.815)	−0.81 (0.33)	0.016 (0.046)	0.25 (0.07)	<0.001 (0.004)	0.302 (0.377)	0.003 (0.014)
Middle	−0.39 (0.21)	0.070 (0.130)			−0.36 (0.27)	0.183 (0.251)			−0.43 (0.35)	0.218 (0.290)			0.870 (0.879)	
Inner	−0.37 (0.21)	0.077 (0.139)			−0.41 (0.26)	0.121 (0.190)			−0.30 (0.34)	0.381 (0.456)			0.793 (0.836)	
	Caudate													
	All MS				**RRMS**				**PMS**				**PMS vs RRMS**	
	EM (SE)	***p* (FDR-*p*)**	**ES (SE)**	***p* (FDR-*p*)**	**EM (SE)**	***p* (FDR-*p*)**	**ES (SE)**	***p* (FDR-*p*)**	**EM (SE)**	***p* (FDR-*p*)**	**ES (SE)**	***p* (FDR-*p*)**	***p* (FDR-*p*)**	***p* (FDR-*p*)**
MTR														
Outer	−0.45 (0.20)	0.030 (0.070)	0.12 (0.04)	0.007 (0.025)	−0.17 (0.25)	0.489 (0.559)	0.06 (0.05)	0.249 0.322)	−0.94 (0.33)	0.006 (0.024)	0.22 (0.07)	0.002 (0.013)	0.068 (0.128)	0.064 (0.124)
Middle	−0.34 (0.19)	0.091 (0.159)			−0.14 (0.24)	0.573 (0.640)			−0.68 (0.32)	0.039 (0.082)			0.183 (0.251)	
Inner	−0.21 (0.19)	0.253 (0.322)			−0.05 (0.23)	0.821 (0.857)			−0.49 (0.31)	0.112 (0.188)			0.255 (0.322)	

Continued

Table 2 Mean Estimated MTR and R2* Layer-Specific Z-Scores and CSF-In Z-Score Change per Layer in Patients With Multiple Sclerosis, as a Whole and According to Disease Phenotype, in Cortex, Thalamus, and Caudate *(continued)*

	Caudate											
	All MS			RRMS			PMS			PMS vs RRMS		
	EM (SE)	*p* (FDR-*p*)	ES (SE)	*p* (FDR-*p*)	EM (SE)	*p* (FDR-*p*)	ES (SE)	*p* (FDR-*p*)	EM (SE)	*p* (FDR-*p*)	ES (SE)	*p* (FDR-*p*)	*p* (FDR-*p*)
R2*													
Outer	0.21 (0.18)	0.250 (0.322)	0.10 (0.04)	0.010 (0.031)	−0.11 (0.22)	0.611 (0.674)	0.08 (0.05)	0.120 (0.190)	0.76 (0.29)	0.010 (0.031)	0.14 (0.06)	0.025 (0.061)	0.019 (0.053)	0.389 (0.456)
Middle	0.30 (0.18)	0.107 (0.184)			−0.01 (0.22)	0.950 (0.950)			0.82 (0.29)	0.006 (0.024)			0.024 (0.061)	
Inner	0.41 (0.19)	0.034 (0.077)			0.04 (0.23)	0.866 (0.879)			1.05 (0.29)	0.001 (0.005)			0.009 (0.030)	

Abbreviations: EM = estimated mean; ES = estimated slope; FDR = false-discovery rate; HC = healthy controls; MS = multiple sclerosis; MTR = magnetization transfer ratio; PMS = progressive multiple sclerosis; RRMS = relapsing-remitting multiple sclerosis; SE = standard error.
Mean estimated layer-specific z-scores, related standard errors, and *p*-values testing the null hypothesis that mean z-score equals zero (i.e., healthy population expected value) in each group. Estimates, standard errors, and *p*-values for slopes (i.e., mean CSF-in z-score changes per layer whose significantly nonzero values are suggestive of a CSF-in gradient of microstructural abnormalities) are reported. *p*-values of between-group comparisons are also provided. Analyses were performed using linear mixed models. FDR correction (Benjamini-Hochberg procedure) was applied to account for the overall number of tests.

In the thalamus, compared with controls, patients with MS showed significantly lower MTR and R2* only in the outer layers (FDR-p = 0.016 and 0.030, respectively). A significant CSF-in z-score change per layer only of thalamic MTR was found (FDR-p = 0.002) because of a more pronounced deviation of thalamic MTR from age-specific and sex-specific expected values closer to the CSF (Table 2, Figure 3).

In the caudate, compared with HC, MS showed no significant difference in both MTR and R2* of all the 3 layers (FDR-$p \geq 0.070$). However, we found a significant CSF-in z-score change per layer of MTR and R2* (FDR-p = 0.025 and 0.031, respectively), with a significant trend of larger MTR reduction closer to CSF and R2* increase moving away from the CSF (Table 2, Figure 3).

MTR and R2* Z-Scores in Cortical, Thalamic, and Caudate Layers in MS Phenotypes

In the cortex, compared with HC, patients with RRMS showed significantly lower MTR in the outer layer (FDR-p = 0.025), as well as significantly lower R2* in all the 3 layers (all FDR-$p \leq 0.016$), while PMS showed significantly reduced MTR in the outer (FDR-$p < 0.001$) and middle (FDR-p = 0.016) layers, as well as significantly decreased R2* only in the outer layer (FDR-p = 0.003). In the direct comparison, no significant difference between PMS and RRMS was found (FDR-$p \geq 0.098$). We found a significant cortical CSF-in z-score change per layer in both RRMS and PMS (FDR-p = 0.002 and FDR-$p < 0.001$, respectively), without significant between-group difference. A significant CSF-in gradient of alteration of cortical R2*, with lower values closer to CSF, was found only in PMS (FDR-p = 0.005), with a significant between-phenotype effect (FDR-p = 0.030) (Table 2, Figure 4).

In the thalamus, compared with HC, RRMS showed no significant differences in both MTR and R2* of all the 3 layers (FDR-$p \geq 0.190$), whereas PMS showed significantly lower MTR in the outer (FDR-p = 0.016) and middle layers (FDR-p = 0.048), as well as significantly lower R2* only in the outer layer (FDR-p = 0.046). In the direct comparison, no significant difference between PMS and RRMS was found (FDR-$p \geq 0.209$). A significant CSF-in z-score change per layer of thalamic MTR was found in both RRMS and PMS (FDR-p = 0.042 and FDR-p = 0.005, respectively), without significant between-group difference. A significant CSF-in gradient of alteration of thalamic R2*, with lower values closer to CSF, was found only in PMS (FDR-p = 0.004), with a significant between-phenotypes effect (FDR-p = 0.014) (Table 2, Figure 4).

In the caudate, compared with HC, RRMS showed no significant difference in both MTR and R2* of all the 3 layers (FDR-$p \geq$ 0.559), whereas PMS showed significantly lower MTR in the outer layer (FDR-p = 0.024), as well as significantly higher R2* in all the 3 layers (all FDR-$p \leq 0.031$). In the direct comparison, a significant higher R2* in the inner layer was found in PMS

Figure 3 MTR and R2* Z-Score Distribution in Cortical, Thalamic, and Caudate Layers in All Patients With Multiple Sclerosis

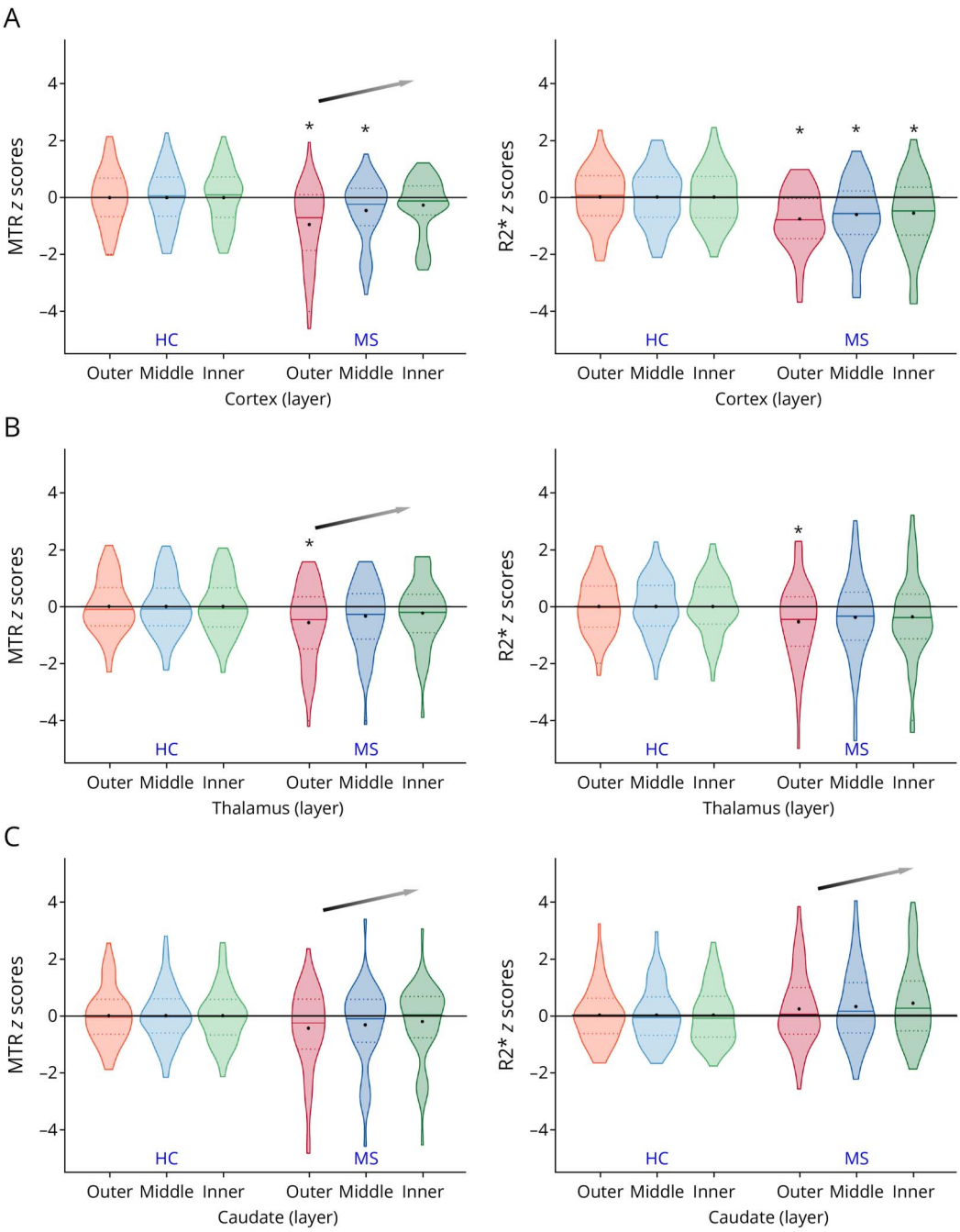

Violin plots show the distribution of MTR and R2* z-scores in (A) cortex, (B) thalamus, and (C) caudate in the outer, middle, and inner layers in patients with multiple sclerosis. Healthy controls are only shown as a reference group for illustrative purposes. The symbol (*) indicates layers with a significantly nonzero (i.e., healthy population expected value) mean estimated z-score. Arrows denote significantly nonzero estimated slopes (i.e., mean CSF-in z-score changes per layer), suggestive of a CSF-in gradient of microstructural abnormalities. FDR correction (Benjamini-Hochberg procedure) was applied. See main text and Table 2 for further details. HC = healthy controls; MS = multiple sclerosis; MTR = magnetization transfer ratio.

compared with RRMS (FDR-p = 0.030). A significant CSF-in z-score change per layer of MTR values in the caudate was found only in PMS (FDR-p = 0.013), although without significant between-phenotypes difference (Table 2, Figure 4).

Analysis of Associations

No significant correlations were found between MTR and R2* in MS as a whole and according to phenotypes, except from the MTR-R2* correlation in the outer cortical layer in the whole MS group (r = 0.44, FDR-p = 0.04) (eTable 1).

In the whole MS group, lower cortical MTR in the outer layer significantly associated with older age (FDR-p = 0.027) and lower cortical thickness (FDR-p = 0.023). Decreased MTR in the outer and middle cortical layers significantly associated with lower normalized brain volume (FDR-p ≤ 0.018),

Figure 4 MTR and R2* Z-Score Distribution in Cortical, Thalamic, and Caudate Layers in Patients With Multiple Sclerosis, According to Their Clinical Phenotype

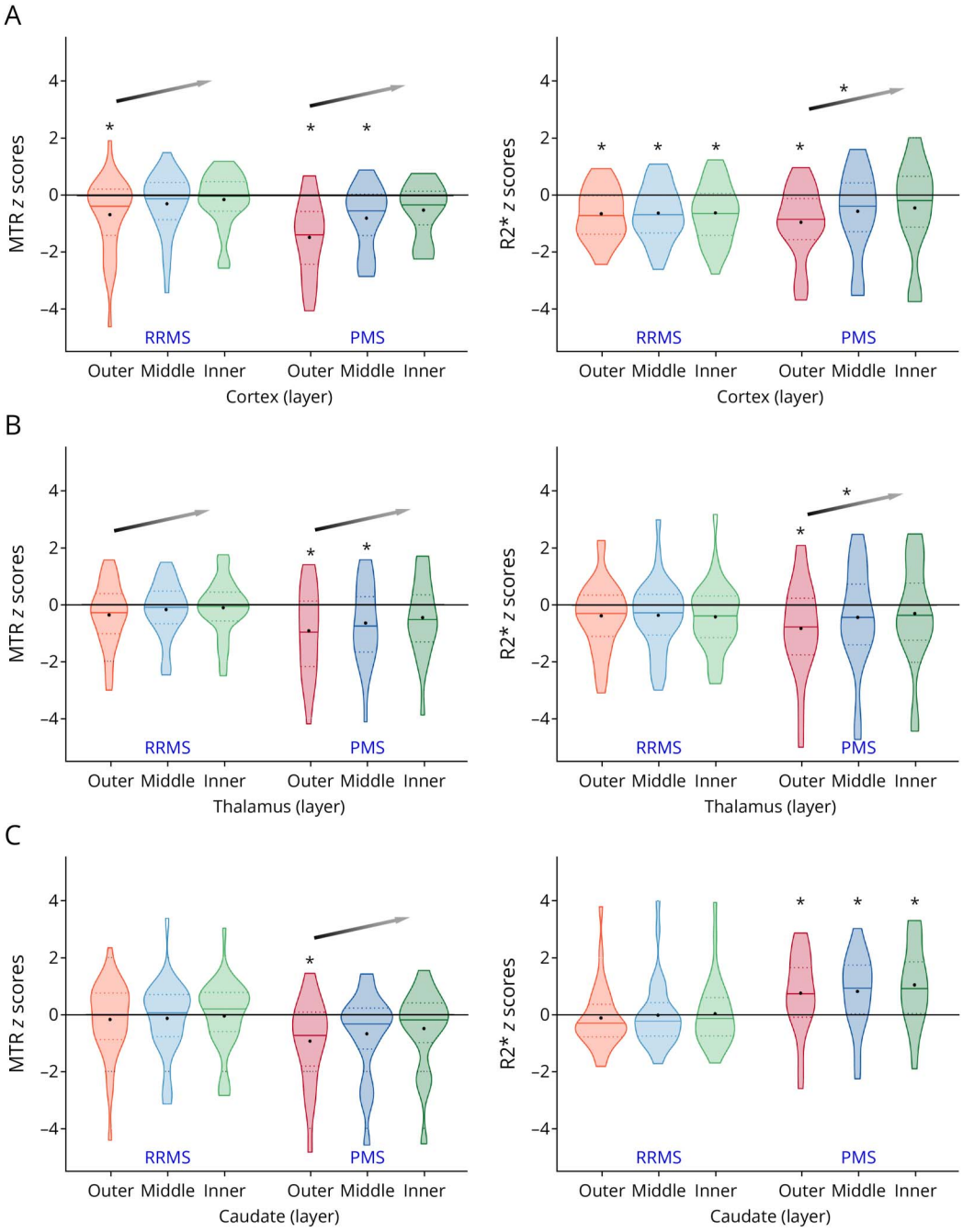

Violin plots show the distribution of MTR and R2* z-scores in (A) cortex, (B) thalamus, and (C) caudate in the outer, middle, and inner layers in relapsing-remitting and progressive multiple sclerosis. The symbol (*) indicates layers with a significantly nonzero (i.e., healthy population expected value) mean estimated z-score. Arrows denote significantly nonzero estimated slopes (i.e., mean CSF-in z-score changes per layer), suggestive of a CSF-in gradient of microstructural abnormalities. The symbol (*) above arrows marks significant differences in slopes between phenotypes (linear mixed models). FDR correction (Benjamini-Hochberg procedure) was applied. See main text and Table 2 for further details. MTR = magnetization transfer ratio; PMS = progressive multiple sclerosis; RRMS = relapsing-remitting multiple sclerosis.

whereas lower MTR in all 3 layers significantly associated with higher WM lesion volume (FDR-$p \leq 0.027$). A steeper cortical MTR gradient in the CSF-in direction significantly associated with older age (FDR-$p = 0.016$), higher WM lesion volume (FDR-$p = 0.016$), lower normalized brain volume (FDR-$p < 0.001$), and lower cortical thickness (FDR-$p = 0.016$). Decreased R2* in the outer cortical layer significantly associated with lower normalized brain volume (FDR-$p = 0.027$), whereas the steeper CSF-in cortical gradient of R2* significantly associated with lower cortical thickness (FDR-$p = 0.027$) (Table 3). No significant associations were found between cortical MTR and R2* and cortical lesion volume.

Table 3 Associations of MTR and R2* Layer-Specific Z-Scores and CSF-In Z-Score Changes per Layer With Demographic, Clinical, and Conventional MRI Metrics in Patients With Multiple Sclerosis in Cortex, Thalamus, and Caudate

	Cortex							
	MTR				R2*			
	β^a (SE)	*p* (FDR-*p*)	β^b (SE)	*p* (FDR-*p*)	β^a (SE)	*p* (FDR-*p*)	β^b (SE)	*p* (FDR-*p*)
Age ($\times 10^{-1}$)								
Outer	−0.60 (0.18)	0.002 (0.027)	0.18 (0.05)	<0.001 (0.016)	−0.27 (0.15)	0.082 (0.255)	0.05 (0.05)	0.264 (0.469)
Middle	−0.40 (0.15)	0.013 (0.09)			−0.18 (0.17)	0.301 (0.517)		
Inner	−0.24 (0.14)	0.087 (0.262)			−0.16 (0.19)	0.391 (0.598)		
DD ($\times 10^{-1}$)								
Outer	−0.42 (0.17)	0.015 (0.095)	0.09 (0.05)	0.058 (0.200)	−0.21 (0.13)	0.117 (0.314)	0.00 (0.04)	0.967 (0.967)
Middle	−0.33 (0.13)	0.018 (0.099)			−0.20 (0.15)	0.184 (0.420)		
Inner	−0.24 (0.12)	0.053 (0.197)			−0.20 (0.16)	0.210 (0.423)		
EDSS								
Outer	−0.23 (0.08)	0.009 (0.073)	0.06 (0.02)	0.014 (0.091)	−0.09 (0.07)	0.195 (0.420)	0.05 (0.02)	0.011 (0.085)
Middle	−0.15 (0.07)	0.028 (0.128)			−0.01 (0.08)	0.868 (0.940)		
Inner	−0.11 (0.06)	0.078 (0.249)			0.01 (0.08)	0.880 (0.941)		
WMLV								
Outer	−0.52 (0.11)	<0.001 (0.002)	0.12 (0.03)	0.001 (0.016)	−0.23 (0.10)	0.027 (0.128)	0.04 (0.03)	0.195 (0.420)
Middle	−0.37 (0.10)	<0.001 (0.011)			−0.14 (0.12)	0.243 (0.450)		
Inner	−0.28 (0.09)	0.002 (0.027)			−0.15 (0.13)	0.256 (0.460)		
CLV								
Outer	−1.13 (0.92)	0.227 (0.428)	0.33 (0.25)	0.194 (0.420)	−1.51 (0.68)	0.031 (0.140)	0.05 (0.21)	0.816 (0.916)
Middle	−0.65 (0.75)	0.390 (0.598)			−1.24 (0.78)	0.118 (0.314)		
Inner	−0.46 (0.66)	0.483 (0.692)			−1.41 (0.85)	0.104 (0.289)		
NBV ($\times 10^{-2}$)								
Outer	1.55 (0.29)	<0.001 (<0.001)	−0.48 (0.07)	<0.001 (<0.001)	0.81 (0.25)	0.002 (0.027)	−0.10 (0.08)	0.249 (0.456)
Middle	0.92 (0.26)	<0.001 (0.018)			0.61 (0.30)	0.047 (0.175)		
Inner	0.60 (0.24)	0.017 (0.099)			0.62 (0.33)	0.064 (0.212)		
Cth								
Outer	6.86 (2.02)	0.001 (0.023)	−2.42 (0.51)	<0.001 (0.001)	0.92 (1.69)	0.589 (0.782)	−1.51 (0.46)	0.002 (0.027)
Middle	3.99 (1.71)	0.024 (0.119)			−1.63 (1.90)	0.393 (0.598)		
Inner	2.01 (1.55)	0.199 (0.420)			−2.10 (2.06)	0.313 (0.528)		
NCPV ($\times 10^{-2}$)								
Outer	−0.01 (0.03)	0.712 (0.86)	0.02 (0.01)	0.079 (0.249)	0.02 (0.03)	0.409 (0.608)	0.01 (0.01)	0.500 (0.701)
Middle	0.01 (0.03)	0.777 (0.888)			0.03 (0.03)	0.317 (0.528)		
Inner	0.02 (0.03)	0.397 (0.600)			0.03 (0.03)	0.330 (0.533)		
	Thalamus							
	MTR				R2*			
	β^a (SE)	*p* (FDR-*p*)	β^b (SE)	*p* (FDR-*p*)	β^a (SE)	*p* (FDR-*p*)	β^b (SE)	*p* (FDR-*p*)
Age ($\times 10^{-1}$)								

Continued

Table 3 Associations of MTR and R2* Layer-Specific Z-Scores and CSF-In Z-Score Changes per Layer With Demographic, Clinical, and Conventional MRI Metrics in Patients With Multiple Sclerosis in Cortex, Thalamus, and Caudate *(continued)*

	Thalamus							
	MTR				R2*			
	β[a] (SE)	*p* (FDR-*p*)	β[b] (SE)	*p* (FDR-*p*)	β[a] (SE)	*p* (FDR-*p*)	β[b] (SE)	*p* (FDR-*p*)
Outer	−0.29 (0.19)	0.140 (0.354)	0.09 (0.04)	0.036 (0.149)	−0.26 (0.20)	0.202 (0.420)	0.06 (0.05)	0.220 (0.426)
Middle	−0.17 (0.17)	0.319 (0.528)			−0.21 (0.22)	0.326 (0.530)		
Inner	−0.11 (0.17)	0.499 (0.701)			−0.15 (0.21)	0.487 (0.692)		
DD (×10^{-1})								
Outer	−0.13 (0.17)	0.430 (0.634)	0.08 (0.03)	0.019 (0.100)	−0.35 (0.17)	0.046 (0.175)	−0.02 (0.04)	0.570 (0.771)
Middle	−0.02 (0.15)	0.918 (0.943)			−0.44 (0.18)	0.017 (0.099)		
Inner	0.03 (0.14)	0.826 (0.917)			−0.40 (0.18)	0.028 (0.128)		
EDSS								
Outer	−0.16 (0.08)	0.056 (0.200)	0.04 (0.02)	0.046 (0.175)	−0.18 (0.09)	0.041 (0.163)	0.05 (0.02)	0.009 (0.073)
Middle	−0.12 (0.07)	0.095 (0.273)			−0.12 (0.09)	0.213 (0.423)		
Inner	−0.09 (0.07)	0.227 (0.428)			−0.08 (0.09)	0.402 (0.604)		
WM LV								
Outer	−0.16 (0.13)	0.209 (0.423)	0.06 (0.03)	0.018 (0.099)	−0.37 (0.13)	0.007 (0.070)	0.07 (0.03)	0.035 (0.148)
Middle	−0.08 (0.12)	0.474 (0.691)			−0.31 (0.14)	0.033 (0.141)		
Inner	−0.03 (0.11)	0.764 (0.888)			−0.23 (0.14)	0.103 (0.289)		
TLV								
Outer	−1.63 (1.31)	0.219 (0.426)	0.12 (0.28)	0.665 (0.829)	0.51 (1.43)	0.724 (0.869)	1.05 (0.29)	0.001 (0.016)
Middle	−1.52 (1.16)	0.197 (0.420)			1.96 (1.48)	0.191 (0.420)		
Inner	−1.38 (1.13)	0.227 (0.428)			2.60 (1.43)	0.075 (0.245)		
NBV (×10^{-2})								
Outer	0.73 (0.33)	0.033 (0.141)	−0.23 (0.07)	0.002 (0.024)	0.36 (0.37)	0.334 (0.534)	−0.16 (0.08)	0.062 (0.208)
Middle	0.49 (0.30)	0.112 (0.306)			0.21 (0.39)	0.591 (0.782)		
Inner	0.28 (0.30)	0.358 (0.564)			0.05 (0.38)	0.896 (0.941)		
NTV								
Outer	0.25 (0.09)	0.006 (0.059)	−0.05 (0.02)	0.012 (0.087)	0.10 (0.10)	0.324 (0.530)	−0.05 (0.02)	0.014 (0.091)
Middle	0.19 (0.08)	0.019 (0.100)			0.04 (0.10)	0.671 (0.831)		
Inner	0.15 (0.08)	0.058 (0.200)			−0.01 (0.10)	0.926 (0.946)		
NCPV (×10^{-2})								
Outer	0.00 (0.04)	0.910 (0.942)	0.01 (0.01)	0.486 (0.692)	−0.01 (0.04)	0.769 (0.888)	0.01 (0.01)	0.361 (0.564)
Middle	0.01 (0.03)	0.663 (0.829)			−0.01 (0.04)	0.897 (0.941)		
Inner	0.01 (0.03)	0.653 (0.825)			0.00 (0.04)	0.934 (0.949)		
	Caudate							
	MTR				**R2***			
	β[a] (SE)	*p* (FDR-*p*)	β[b] (SE)	*p* (FDR-*p*)	β[a] (SE)	*p* (FDR-*p*)	β[b] (SE)	*p* (FDR-*p*)
Age (×10^{-1})								

Continued

Table 3 Associations of MTR and R2* Layer-Specific Z-Scores and CSF-In Z-Score Changes per Layer With Demographic, Clinical, and Conventional MRI Metrics in Patients With Multiple Sclerosis in Cortex, Thalamus, and Caudate *(continued)*

	Caudate							
	MTR				R2*			
	β[a] (SE)	*p* (FDR-*p*)	β[b] (SE)	*p* (FDR-*p*)	β[a] (SE)	*p* (FDR-*p*)	β[b] (SE)	*p* (FDR-*p*)
Outer	−0.30 (0.21)	0.149 (0.372)	0.02 (0.04)	0.632 (0.820)	0.03 (0.19)	0.872 (0.940)	0.06 (0.04)	0.157 (0.386)
Middle	−0.27 (0.20)	0.189 (0.420)			0.10 (0.19)	0.596 (0.783)		
Inner	−0.26 (0.19)	0.176 (0.412)			0.14 (0.20)	0.475 (0.691)		
DD (×10^{-1})								
Outer	−0.24 (0.18)	0.180 (0.417)	0.02 (0.04)	0.682 (0.839)	−0.10 (0.16)	0.540 (0.740)	0.02 (0.03)	0.513 (0.709)
Middle	−0.2 (0.17)	0.268 (0.472)			−0.09 (0.16)	0.589 (0.782)		
Inner	−0.21 (0.17)	0.203 (0.420)			−0.06 (0.17)	0.741 (0.873)		
EDSS								
Outer	−0.26 (0.08)	0.004 (0.040)	0.05 (0.02)	0.008 (0.072)	0.13 (0.08)	0.127 (0.329)	0.01 (0.02)	0.625 (0.816)
Middle	−0.19 (0.08)	0.026 (0.128)			0.11 (0.08)	0.175 (0.412)		
Inner	−0.16 (0.08)	0.057 (0.200)			0.14 (0.08)	0.095 (0.273)		
WM LV								
Outer	−0.48 (0.13)	<0.001 (0.011)	0.08 (0.03)	0.003 (0.033)	−0.04 (0.13)	0.740 (0.873)	0.04 (0.03)	0.089 (0.264)
Middle	−0.34 (0.13)	0.010 (0.081)			0.01 (0.13)	0.948 (0.958)		
Inner	−0.31 (0.12)	0.015 (0.095)			0.05 (0.13)	0.730 (0.870)		
CaLV								
Outer	−0.87 (2.84)	0.761 (0.888)	−0.17 (0.59)	0.774 (0.888)	−0.52 (2.55)	0.839 (0.926)	0.60 (0.52)	0.256 (0.460)
Middle	−1.04 (2.73)	0.706 (0.858)			0.33 (2.54)	0.897 (0.941)		
Inner	−1.21 (2.60)	0.644 (0.824)			0.67 (2.65)	0.800 (0.909)		
NBV (×10^{-2})								
Outer	0.41 (0.38)	0.281 (0.49)	−0.12 (0.08)	0.119 (0.314)	−0.35 (0.34)	0.313 (0.528)	0.00 (0.07)	0.964 (0.967)
Middle	0.22 (0.37)	0.545 (0.743)			−0.22 (0.34)	0.511 (0.709)		
Inner	0.17 (0.35)	0.636 (0.820)			−0.34 (0.35)	0.341 (0.542)		
NCV								
Outer	0.08 (0.18)	0.648 (0.824)	−0.05 (0.04)	0.137 (0.352)	−0.19 (0.16)	0.233 (0.434)	−0.05 (0.03)	0.166 (0.399)
Middle	−0.02 (0.17)	0.893 (0.941)			−0.22 (0.16)	0.164 (0.399)		
Inner	−0.03 (0.16)	0.866 (0.940)			−0.28 (0.16)	0.087 (0.262)		
NCPV (×10^{-2})								
Outer	−0.01 (0.04)	0.913 (0.942)	0.01 (0.01)	0.212 (0.423)	−0.01 (0.04)	0.862 (0.940)	0.01 (0.01)	0.288 (0.499)
Middle	0.01 (0.04)	0.812 (0.916)			0.00 (0.04)	0.909 (0.942)		
Inner	0.02 (0.04)	0.689 (0.842)			0.01 (0.04)	0.824 (0.917)		

Abbreviations: CLV = cortical lesion volume; CaLV = caudate lesion volume; Cth = cortical thickness; DD = disease duration; EDSS = Expanded Disability Status Scale; EM = estimated mean; FDR = false-discovery rate; HC = healthy controls; LV = lesion volume; MTR = magnetization transfer ratio; NBV = normalized brain volume; NCPV = normalized choroid plexus volume; NCV = normalized caudate volume; NTV = normalized thalamic volume; PMS = progressive multiple sclerosis; RRMS = relapsing-remitting multiple sclerosis; SE = standard error; TLV = thalamic lesion volume; WM = white matter.
Beta-coefficients (β) related to standard errors and *p* values from linear mixed models are reported. The analysis for lesion volumes was performed on square-root-transformed values. FDR correction (Benjamini-Hochberg procedure) was applied to account for the overall number of tests.
[a] β regression coefficient, quantifying the estimated mean change in the layer-specific z-score, associated with a one-unit increase in the predictor.
[b] β regression coefficient, quantifying the estimated mean change in the CSF-in z-score change per layer, associated with a one-unit increase in the predictor.

The steeper CSF-in thalamic MTR gradient significantly associated with lower normalized brain volume (FDR-p = 0.024), whereas the steeper R2* thalamic gradient significantly associated with higher thalamic lesion volume (FDR-p = 0.016) (Table 3).

In the caudate, lower MTR in the outer layer significantly associated with higher EDSS (FDR-p = 0.040) and higher WM lesion volume (FDR-p = 0.011), whereas the steeper CSF-in MTR gradient significantly associated with higher WM lesion volume (FDR-p = 0.033). No significant associations were found between caudate MTR and R2* and caudate lesion volume (Table 3). MTR and R2* of the different GM layers and their gradient of CSF-in damage were also significantly associated with other clinical and structural MRI measures but did not survive correction for multiple comparisons (Table 3).

No significant associations were found with CP volumes (FDR-$p \geq 0.499$).

The analysis of associations in the RRMS and PMS groups separately was similar to those found in the whole MS group, with no evidence of significant between-group differences (eTable 2).

Discussion

By exploring the CSF-in gradient of damage in the cortex, thalamus, and caudate of patients with MS using MTR and R2*, our study showed that different patterns of abnormalities can be detected in these 3 GM structures, especially in the outer layers. These alterations were more severe in PMS and correlated with more severe clinical disability and structural MRI measures of brain damage.

Since GM MTR has been suggested to reflect mainly myelin density,[22,23] whereas R2* is known to be influenced by both iron and myelin content,[20,21] the combined analyses of MTR and R2* in HC allowed us to explore the dynamic changes of these substrates in different GM structures across lifespan. The obtained trajectories were used to investigate how MS-related pathologic processes affect to a different extent the different CSF-adjacent GM structures after removing the physiologic effects of sex and aging.

The analysis of MTR and R2* trajectories across lifespan in HC demonstrated a gradual increase of thalamic MTR until mid-age, reflecting the physiologic myelination process occurring mainly in the first life decades, with the highest myelin density around 40s.[34] Although a trend of thalamic R2* increase was observed in the first decades, no significant changes were detected through lifespan. This is consistent with previous findings[13,35] showing a steeper increase of thalamic iron content until the late 30s, increasing only gradually thereafter.[13] Moreover, since the thalamus has low iron content compared with other deep GM nuclei, this could explain its relatively minor R2* changes.[13] Cortical and caudate R2*, instead, linearly increased with age, with a steeper slope in the caudate.[13,35-38] In the deep GM nuclei constituting the striatum, neurodegenerative processes characterized by iron accumulation have been demonstrated in physiologic aging,[16,17,19] due to their higher susceptibility to iron metabolism dysregulation[39] and higher astrocytes density.[15-17] Indeed, even after the myelinating process accomplishment, with no further iron accumulation in oligodendrocytes,[16] microglia and astrocytes continue to store iron during adulthood and senescence.[15,16,40] These processes may explain the elevated iron levels found post mortem in the basal ganglia (except for the thalamus),[39] and the age-related susceptibility increase on quantitative susceptibility mapping.[13] A similar age-related iron accumulation process occurs in the cortex, especially in the motor and frontal regions, which are functionally linked to the deep GM nuclei circuits and may undergo similar ageing-induced neurodegenerative processes.[16,17] Conversely, no significant changes in cortical and caudate MTR were observed through lifespan. Although a previous study showed MTR decrease after the age of 40,[34] discrepancies may be partially due to younger mean age, differences in MRI acquisitions (3T vs 1.5T), and analysis performed in our HC group.[34] Since these structures are less myelinated than the thalamus,[18] with aging they may undergo a physiologic senescence-induced neurodegenerative process characterized by neuronal energetic failure[41] and synaptic loss,[42] rather than myelin loss, which may appear later from the fifth/sixth decades.

Aside from age-related physiologic variations, a CSF-in gradient was found in healthy brain only for MTR predominantly in the cortex[9] but also in thalamus.[8] This is probably due to the tissue histologic structure because the subpial cortex is characterized by higher density of unmyelinated neurites and small neurons.[14] Conversely, a mild layer effect in iron content, measured by R2*, was detected only in the caudate. Such physiologic cytoarchitectural layer-dependent variability still needs to be explored; therefore, our findings provide interesting insights into caudate histologic composition, needing pathologic confirmation. Clearly, the application of different methods to identify layers within distinct GM structures and removing the outermost layer for the thalamus and caudate may also contribute to explain variability among GM structures.

In patients with MS, our results support the hypothesis of a CSF-driven pathologic process that is heterogeneous in the 3 GM structures explored.[2,4,7-9,11,12] In the cortex, compared with HC, MTR was significantly lower in the outer layer in both phenotypes, with abnormalities being more severe and involving also the middle cortical layer in PMS. Moreover, a cortical CSF-in MTR gradient was present in both MS groups. Our findings support pathologic[1,2,4] and MRI data[9,43] showing that subpial demyelination occurs from the earliest MS phases and accumulates with progression. We also found a

significantly lower R2* in all 3 cortical layers in RRMS but only in the outer layer in PMS, with a CSF-in gradient of cortical R2* alteration reflecting lower values closer to CSF only in PMS. These results are in line with previous studies showing lower R2*[44] and higher T2* mainly in subpial layers.[6,7] However, differently from a previous 7T T2* study,[6] we found that R2* abnormalities in PMS were not diffuse to the entire cortical ribbon but involved only the outer layer. Differences in the cohort of patients with MS explored, in scanner field strengths, MRI sequences, and in the methods applied may contribute to explain, at least partially, these discrepancies. Globally, our results suggest that both lower R2* and MTR especially in outer cortical layers may reflect iron loss due to demyelination and oligodendrocytes loss.[6,7,44] The presence of iron-rich activated microglia[15,16,45] and neurodegenerative processes associated with iron accumulation, especially in PMS and in inner cortical layers, may counterbalance myelin loss, thus increasing R2*.[45-47]

Compared with HC, we found both lower MTR and R2* in the outer thalamic layer, together with a CSF-in damage gradient, with lower CSF-adjacent MTR and R2*. Although such abnormalities were significant only in PMS, no difference between PMS and RRMS was found in the direct comparisons, except for a CSF-in gradient of thalamic R2*. Heterogeneous pathologic processes may affect the thalamus,[2,3,40,48] with a CSF-in pathologic gradient of demyelination, neuroaxonal loss, and activated microglia especially in PMS.[2] By showing both lower MTR and R2*, our study confirms previous pathologic[2] and MRI findings[5,8,49] suggesting that demyelination and iron loss[5,49-52] in the outer thalamic layer may occur since the earliest MS phases and involve also deeper layers with progression. In RRMS, the lack of MTR and R2* difference may be secondary to a milder loss of myelin and oligodendrocyte-associated iron that may also be counterbalanced by an increased density of iron-rich activated microglia.[2] Conversely, in PMS, demyelination and oligodendrocyte loss may be relatively more substantial than the amount of activated microglia and iron accumulation associated with neurodegeneration,[49,50] thus promoting a significant R2* decrease.[2]

Of interest, in the caudate, we found different MTR and R2* patterns compared with the thalamus. Although further studies are necessary to confirm our findings, this may be explained by their different cytoarchitectures with possible differences in tissue susceptibility to MS-related pathologic processes. A significantly lower MTR in the outer caudate layer and higher R2* in all 3 layers were found only in PMS. Although pathologic studies showed that focal demyelination may also affect the caudate, especially in periventricular areas,[3,48] our MTR results suggest a more limited CSF-in gradient of myelin loss in this structure compared with the thalamus, being evident only in advanced disease phases. A higher R2* in all caudate layers aligns with previous studies showing iron accumulation in MS patients' striatum, especially in PMS.[49,50] Although the mechanisms underlying iron accumulation within the caudate are still unclear, several processes are likely to co-occur: the striatum is particularly rich in iron, thus is susceptible to iron regulatory mechanisms disruption and neuronal death, as commonly observed in neurodegenerative disorders.[39] Moreover, also in this structure, iron accumulation/redistribution may be secondary to a higher concentration of activated microglia/macrophages and a higher neuronal iron uptake to enhance mitochondrial genesis in the presence of oxidative stress.[45]

The analysis of associations showed that clinical disability and structural brain damage were mainly associated with MTR and R2* of the outer layers of all 3 structures, as well as with a steeper CSF-in damage gradient, although only a few associations survived correction for multiple comparisons. Our results are consistent with pathologic[4] and MRI studies[6,8] supporting the contribution of a CSF-in damage gradient in determining the accumulation of focal lesions, brain atrophy, and clinical disability. Notably, the lack of significant structure-specific and layer-specific correlations between MTR and R2* in patients with MS supports their combined evaluation because they reflect different pathologic processes; thus, our multiparametric evaluation may better characterize CSF-in gradient of damage in MS.

Disappointingly, no association between CSF-in gradient measures and CP enlargement was found. Since CP enlargement has been described from the earliest phases of MS and remains relatively stable throughout the disease course,[24-26] it may represent an early marker of chronic inflammation that reaches a ceiling effect over time.

The study has some limitations. First, we evaluated 2 relatively small cohorts of HC and patients with MS, not exploring possible differences according to disease duration, clinical disability, or primary-progressive/secondary-progressive course. Second, high-field MRI does not provide the spatial resolution of ultra-high-field scanners, both in assessment of microstructural damage distribution and in lesion identification. In this regard, although we applied published recommendations for lesion assessment, manual detection of these lesions on 3T scans might have some intrinsic bias and be less sensitive compared with ultra-high-field scans or pathologic evaluation. We explored cortical, thalamic, and caudate layers at a global level, not evaluating specific damage patterns at the regional level, which may provide further information on underlying pathophysiologic mechanisms and consequent contribution to clinical impairment. Although the hippocampus could be another relevant GM region in direct contact with the CSF, frequently affected by MS, the evaluation of a CSF-in gradient of damage of this structure is challenging because of its convoluted macroscopical structure and its reduced thickness. Finally, the retrospective design of our study might have introduced some confounding effects. Future prospective, longitudinal studies are needed to evaluate the structure-specific microstructural damage trajectories and their associations with disease evolution.

In conclusion, the concomitant assessment of MTR and R2* in the cortex, thalamus, and caudate allowed us to detect heterogeneous and structure-specific gradients of microstructural alterations related to CSF-proximity, in CSF-in demyelination in these 3 structures occurring in all phases of the disease, but becoming more severe in PMS, and of diffuse iron accumulation in the caudate being evident in PMS. These alterations are significantly associated with structural brain damage and may contribute to disability progression throughout disease course.

Study Funding

The authors report no targeted funding.

Disclosure

E. Pagani received speakers' honoraria from Biogen Idec. P. Preziosa received speaker honoraria from Roche, Biogen, Novartis, Merck Serono, Bristol Myers Squibb, Genzyme, Horizon, and Sanofi. He has received research support from Italian Ministry of Health and Fondazione Italiana Sclerosi Multipla. L. Storelli declared the receipt of grants and contracts from FISM-Fondazione Italiana Sclerosi Multipla-within a fellowship program (cod. 2019/BR/009). M. Margoni reports grants and personal fees from Sanofi Genzyme, Merck Serono, Novartis, and Almiral. She was awarded a MAGNIMS-ECTRIMS fellowship in 2020. M. Filippi is Editor-in-Chief of the *Journal of Neurology*, Associate Editor of *Human Brain Mapping*, *Neurological Sciences*, and *Radiology*; received compensation for consulting services from Alexion, Almirall, Biogen, Merck, Novartis, Roche, Sanofi; speaking activities from Bayer, Biogen, Celgene, Chiesi Italia SpA, Eli Lilly, Genzyme, Janssen, Merck-Serono, Neopharmed Gentili, Novartis, Novo Nordisk, Roche, Sanofi, Takeda, and TEVA; participation in Advisory Boards for Alexion, Biogen, Bristol-Myers Squibb, Merck, Novartis, Roche, Sanofi, Sanofi-Aventis, Sanofi-Genzyme, Takeda; scientific direction of educational events for Biogen, Merck, Roche, Celgene, Bristol-Myers Squibb, Lilly, Novartis, Sanofi-Genzyme; he receives research support from Biogen Idec, Merck-Serono, Novartis, Roche, the Italian Ministry of Health, the Italian Ministry of University and Research, and Fondazione Italiana Sclerosi Multipla. M.A. Rocca received consulting fees from Biogen, Bristol Myers Squibb, Eli Lilly, Janssen, and Roche; and speaker honoraria from AstraZaneca, Biogen, Bristol Myers Squibb, Bromatech, Celgene, Genzyme, Horizon Therapeutics Italy, Merck Serono SpA, Novartis, Roche, Sanofi, and Teva. She receives research support from the MS Society of Canada, the Italian Ministry of Health, the Italian Ministry of University and Research, and Fondazione Italiana Sclerosi Multipla. She is an Associate Editor for *Multiple Sclerosis and Related Disorders*. The other authors report no disclosures relevant to the manuscript. Go to Neurology.org/NN for full disclosures.

Publication History

Received by *Neurology: Neuroimmunology & Neuroinflammation* October 18, 2023. Accepted in final form April 19, 2024. Submitted and externally peer reviewed. The handling editor was Associate Editor Friedemann Paul, MD.

Appendix Authors

Name	Location	Contribution
Martina Rubin, MD	Neuroimaging Research Unit, Division of Neuroscience; Neurology Unit, IRCCS San Raffaele Scientific Institute; Vita-Salute San Raffaele University, Milan, Italy	Drafting/revision of the manuscript for content, including medical writing for content; major role in the acquisition of data; analysis or interpretation of data
Elisabetta Pagani, MSc	Neuroimaging Research Unit, Division of Neuroscience, IRCCS San Raffaele Scientific Institute, Milan, Italy	Drafting/revision of the manuscript for content, including medical writing for content; analysis or interpretation of data
Paolo Preziosa, MD, PhD	Neuroimaging Research Unit, Division of Neuroscience; Neurology Unit, IRCCS San Raffaele Scientific Institute; Vita-Salute San Raffaele University, Milan, Italy	Drafting/revision of the manuscript for content, including medical writing for content; major role in the acquisition of data; analysis or interpretation of data
Alessandro Meani, MSc	Neuroimaging Research Unit, Division of Neuroscience, IRCCS San Raffaele Scientific Institute, Milan, Italy	Drafting/revision of the manuscript for content, including medical writing for content; analysis or interpretation of data
Loredana Storelli, PhD	Neuroimaging Research Unit, Division of Neuroscience, IRCCS San Raffaele Scientific Institute, Milan, Italy	Drafting/revision of the manuscript for content, including medical writing for content; analysis or interpretation of data
Monica Margoni, MD, PhD	Neuroimaging Research Unit, Division of Neuroscience; Neurology Unit; Neurorehabilitation Unit, IRCCS San Raffaele Scientific Institute, Milan, Italy	Drafting/revision of the manuscript for content, including medical writing for content; major role in the acquisition of data; analysis or interpretation of data
Massimo Filippi, MD	Neuroimaging Research Unit, Division of Neuroscience; Neurology Unit, IRCCS San Raffaele Scientific Institute; Vita-Salute San Raffaele University; Neurorehabilitation Unit; Neurophysiology Service, IRCCS San Raffaele Scientific Institute, Milan, Italy	Drafting/revision of the manuscript for content, including medical writing for content; study concept or design; analysis or interpretation of data
Maria A. Rocca, MD	Neuroimaging Research Unit, Division of Neuroscience; Neurology Unit, IRCCS San Raffaele Scientific Institute; Vita-Salute San Raffaele University, Milan, Italy	Drafting/revision of the manuscript for content, including medical writing for content; study concept or design; analysis or interpretation of data

References

1. Magliozzi R, Howell OW, Nicholas R, et al. Inflammatory intrathecal profiles and cortical damage in multiple sclerosis. *Ann Neurol.* 2018;83(4):739-755. doi:10.1002/ana.25197
2. Magliozzi R, Fadda G, Brown RA, et al. "Ependymal-in" gradient of thalamic damage in progressive multiple sclerosis. *Ann Neurol.* 2022;92(4):670-685. doi:10.1002/ana.26448
3. Haider L, Simeonidou C, Steinberger G, et al. Multiple sclerosis deep grey matter: the relation between demyelination, neurodegeneration, inflammation and iron. *J Neurol Neurosurg Psychiatry*. 2014;85(12):1386-1395. doi:10.1136/jnnp-2014-307712
4. Magliozzi R, Howell OW, Reeves C, et al. A Gradient of neuronal loss and meningeal inflammation in multiple sclerosis. *Ann Neurol.* 2010;68(4):477-493. doi:10.1002/ana.22230
5. Louapre C, Govindarajan ST, Gianni C, et al. Heterogeneous pathological processes account for thalamic degeneration in multiple sclerosis: insights from 7 T imaging. *Mult Scler.* 2018;24(11):1433-1444. doi:10.1177/1352458517726382

6. Mainero C, Louapre C, Govindarajan ST, et al. A gradient in cortical pathology in multiple sclerosis by in vivo quantitative 7 T imaging. *Brain*. 2015;138(Pt 4):932-945. doi:10.1093/brain/awv011
7. Cohen-Adad J, Benner T, Greve D, et al. In vivo evidence of disseminated subpial T2* signal changes in multiple sclerosis at 7 T: a surface-based analysis. *Neuroimage*. 2011;57(1):55-62. doi:10.1016/j.neuroimage.2011.04.009
8. De Meo E, Storelli L, Moiola L, et al. In vivo gradients of thalamic damage in paediatric multiple sclerosis: a window into pathology. *Brain*. 2021;144(1):186-197. doi:10.1093/brain/awaa379
9. Samson RS, Cardoso MJ, Muhlert N, et al. Investigation of outer cortical magnetisation transfer ratio abnormalities in multiple sclerosis clinical subgroups. *Mult Scler*. 2014;20(10):1322-1330. doi:10.1177/1352458514522537
10. Pardini M, Brown JWL, Magliozzi R, Reynolds R, Chard DT. Surface-in pathology in multiple sclerosis: a new view on pathogenesis? *Brain*. 2021;144(6):1646-1654. doi:10.1093/brain/awab025
11. Brown JW, Pardini M, Brownlee WJ, et al. An abnormal periventricular magnetization transfer ratio gradient occurs early in multiple sclerosis. *Brain*. 2017;140(2):387-398. doi:10.1093/brain/aww296
12. Liu Z, Pardini M, Yaldizli O, et al. Magnetization transfer ratio measures in normal-appearing white matter show periventricular gradient abnormalities in multiple sclerosis. *Brain*. 2015;138(Pt 5):1239-1246. doi:10.1093/brain/awv065
13. Treit S, Naji N, Seres P, et al. R2* and quantitative susceptibility mapping in deep gray matter of 498 healthy controls from 5 to 90 years. *Hum Brain Mapp*. 2021;42(14):4597-4610. doi:10.1002/hbm.25569
14. Trampel R, Bazin PL, Pine K, Weiskopf N. In-vivo magnetic resonance imaging (MRI) of laminae in the human cortex. *Neuroimage*. 2019;197:707-715. doi:10.1016/j.neuroimage.2017.09.037
15. Zhang X, Surguladze N, Slagle-Webb B, Cozzi A, Connor JR. Cellular iron status influences the functional relationship between microglia and oligodendrocytes. *Glia*. 2006;54(8):795-804. doi:10.1002/glia.20416
16. Möller HE, Bossoni L, Connor JR, et al. Iron, myelin, and the brain: neuroimaging meets neurobiology. *Trends Neurosciences*. 2019;42(6):384-401. doi:10.1016/j.tins.2019.03.009
17. Pirpamer L, Hofer E, Gesierich B, et al. Determinants of iron accumulation in the normal aging brain. *Neurobiol Aging*. 2016;43:149-155. doi:10.1016/j.neurobiolaging.2016.04.002
18. Dvorak AV, Swift-LaPointe T, Vavasour IM, et al. An atlas for human brain myelin content throughout the adult life span. *Sci Rep*. 2021;11(1):269. doi:10.1038/s41598-020-79540-3
19. Guan X, Guo T, Zhou C, et al. Altered brain iron depositions from aging to Parkinson's disease and Alzheimer's disease: a quantitative susceptibility mapping study. *Neuroimage*. 2022;264:119683. doi:10.1016/j.neuroimage.2022.119683
20. Birkl C, Birkl-Toeglhofer AM, Kames C, et al. The influence of iron oxidation state on quantitative MRI parameters in post mortem human brain. *Neuroimage*. 2020;220:117080. doi:10.1016/j.neuroimage.2020.117080
21. Bagnato F, Hametner S, Boyd E, et al. Untangling the R2* contrast in multiple sclerosis: a combined MRI-histology study at 7.0 Tesla. *PLoS One*. 2018;13(3):e0193839. doi:10.1371/journal.pone.0193839
22. Langkammer C, Krebs N, Goessler W, et al. Susceptibility induced gray-white matter MRI contrast in the human brain. *Neuroimage*. 2012;59(2):1413-1419. doi:10.1016/j.neuroimage.2011.08.045
23. Schmierer K, Scaravilli F, Altmann DR, Barker GJ, Miller DH. Magnetization transfer ratio and myelin in postmortem multiple sclerosis brain. *Ann Neurol*. 2004;56(3):407-415. doi:10.1002/ana.20202
24. Ricigliano VA, Stankoff B. Choroid plexuses at the interface of peripheral immunity and tissue repair in multiple sclerosis. *Curr Opin Neurol*. 2023;36(3):214-221. doi:10.1097/WCO.0000000000001160
25. Ricigliano VAG, Morena E, Colombi A, et al. Choroid plexus enlargement in inflammatory multiple sclerosis: 3.0-T MRI and translocator protein PET evaluation. *Radiology*. 2021;301(1):166-177. doi:10.1148/radiol.2021204426
26. Muller J, Sinnecker T, Wendebourg MJ, et al. Choroid plexus volume in multiple sclerosis vs neuromyelitis optica spectrum disorder: a retrospective, cross-sectional analysis. *Neurol Neuroimmunol Neuroinflamm*. 2022;9(3):e1147. doi:10.1212/NXI.0000000000001147
27. Valverde S, Cabezas M, Roura E, et al. Improving automated multiple sclerosis lesion segmentation with a cascaded 3D convolutional neural network approach. *Neuroimage*. 2017;155:159-168. doi:10.1016/j.neuroimage.2017.04.034
28. Geurts JJ, Roosendaal SD, Calabrese M, et al. Consensus recommendations for MS cortical lesion scoring using double inversion recovery MRI. *Neurology*. 2011;76(5):418-424. doi:10.1212/WNL.0b013e31820a0cc4
29. Fischl B, Dale AM. Measuring the thickness of the human cerebral cortex from magnetic resonance images. *Proc Natl Acad Sci U S A*. 2000;97(20):11050-11055. doi:10.1073/pnas.200033797
30. Pei M, Nguyen TD, Thimmappa ND, et al. Algorithm for fast monoexponential fitting based on auto-regression on linear operations (ARLO) of data. *Magn Reson Med*. 2015;73(2):843-850. doi:10.1002/mrm.25137
31. Greve DN, Fischl B. Accurate and robust brain image alignment using boundary-based registration. *Neuroimage*. 2009;48(1):63-72. doi:10.1016/j.neuroimage.2009.06.060
32. Fadda G, Brown RA, Magliozzi R, et al. A surface-in gradient of thalamic damage evolves in pediatric multiple sclerosis. *Ann Neurol*. 2019;85(3):340-351. doi:10.1002/ana.25429
33. Storelli L, Pagani E, Rubin M, Margoni M, Filippi M, Rocca MA. A fully automatic method to segment choroid plexuses in multiple sclerosis using conventional MRI sequences. *J Magn Reson Imaging*. 2024;59(5):1643-1652. doi:10.1002/jmri.28937
34. Mascalchi M, Toschi N, Ginestroni A, et al. Gender, age-related, and regional differences of the magnetization transfer ratio of the cortical and subcortical brain gray matter. *J Magn Reson Imaging*. 2014;40(2):360-366. doi:10.1002/jmri.24355
35. Betts MJ, Acosta-Cabronero J, Cardenas-Blanco A, Nestor PJ, Düzel E. High-resolution characterisation of the aging brain using simultaneous quantitative susceptibility mapping (QSM) and R2* measurements at 7 T. *Neuroimage*. 2016;138:43-63. doi:10.1016/j.neuroimage.2016.05.024
36. Buijs M, Doan NT, van Rooden S, et al. In vivo assessment of iron content of the cerebral cortex in healthy aging using 7-Tesla T2*-weighted phase imaging. *Neurobiol Aging*. 2017;53:20-26. doi:10.1016/j.neurobiolaging.2016.09.005
37. Li G, Tong R, Zhang M, et al. Age-dependent changes in brain iron deposition and volume in deep gray matter nuclei using quantitative susceptibility mapping. *Neuroimage*. 2023;269:119923. doi:10.1016/j.neuroimage.2023.119923
38. Haacke EM, Miao Y, Liu M, et al. Correlation of putative iron content as represented by changes in R2* and phase with age in deep gray matter of healthy adults. *J Magn Reson Imaging*. 2010;32(3):561-576. doi:10.1002/jmri.22293
39. Ward RJ, Zucca FA, Duyn JH, Crichton RR, Zecca L. The role of iron in brain ageing and neurodegenerative disorders. *Lancet Neurol*. 2014;13(10):1045-1060. doi:10.1016/S1474-4422(14)70117-6
40. Margoni M, Pagani E, Meani A, et al. Exploring in vivo multiple sclerosis brain microstructural damage through T1w/T2w ratio: a multicentre study. *J Neurol Neurosurg Psychiatry*. 2022;93(7):741-752. doi:10.1136/jnnp-2022-328908
41. Minoshima S, Cross DJ, Foster NL, Henry TR, Kuhl DE. Discordance between traditional pathologic and energy metabolic changes in very early Alzheimer's disease: pathophysiological implications. *Ann New York Acad Sci*. 1999;893:350-352. doi:10.1111/j.1749-6632.1999.tb07852.x
42. Scheff SW, Neltner JH, Nelson PT. Is synaptic loss a unique hallmark of Alzheimer's disease? *Biochem Pharmacol*. 2014;88(4):517-528. doi:10.1016/j.bcp.2013.12.028
43. Derakhshan M, Caramanos Z, Narayanan S, Arnold DL, Louis Collins D. Surface-based analysis reveals regions of reduced cortical magnetization transfer ratio in patients with multiple sclerosis: a proposed method for imaging subpial demyelination. *Hum Brain Mapp*. 2014;35(7):3402-3413. doi:10.1002/hbm.22410
44. Wen J, Yablonskiy DA, Luo J, Lancia S, Hildebolt C, Cross AH. Detection and quantification of regional cortical gray matter damage in multiple sclerosis utilizing gradient echo MRI. *Neuroimage Clin*. 2015;9:164-175. doi:10.1016/j.nicl.2015.08.003
45. Williams R, Buchheit CL, Berman NE, LeVine SM. Pathogenic implications of iron accumulation in multiple sclerosis. *J Neurochem*. 2012;120(1):7-25. doi:10.1111/j.1471-4159.2011.07536.x
46. Al-Radaideh A, Athamneh I, Alabadi H, Hbahbih M. Cortical and subcortical morphometric and iron changes in relapsing-remitting multiple sclerosis and their association with white matter T2 lesion load: a 3-Tesla Magnetic Resonance Imaging Study. *Clin Neuroradiol*. 2019;29(1):51-64. doi:10.1007/s00062-017-0654-0
47. Al-Radaideh A, El-Haj N, Hijjawi N. Iron deposition and atrophy in cerebral grey matter and their possible association with serum iron in relapsing-remitting multiple sclerosis. *Clin Imaging*. 2021;69:238-242. doi:10.1016/j.clinimag.2020.09.006
48. Vercellino M, Masera S, Lorenzatti M, et al. Demyelination, inflammation, and neurodegeneration in multiple sclerosis deep gray matter. *J Neuropathol Exp Neurol*. 2009;68(5):489-502. doi:10.1097/NEN.0b013e3181a19a5a
49. Zivadinov R, Tavazzi E, Bergsland N, et al. Brain iron at quantitative MRI is associated with disability in multiple sclerosis. *Radiology*. 2018;289(2):487-496. doi:10.1148/radiol.2018180136
50. Khalil M, Langkammer C, Pichler A, et al. Dynamics of brain iron levels in multiple sclerosis: a longitudinal 3T MRI study. *Neurology*. 2015;84(24):2396-2402. doi:10.1212/WNL.0000000000001679
51. Schweser F, Raffaini Duarte Martins AL, Hagemeier J, et al. Mapping of thalamic magnetic susceptibility in multiple sclerosis indicates decreasing iron with disease duration: a proposed mechanistic relationship between inflammation and oligodendrocyte vitality. *Neuroimage*. 2018;167:438-452. doi:10.1016/j.neuroimage.2017.10.063
52. Schweser F, Hagemeier J, Dwyer MG, et al. Decreasing brain iron in multiple sclerosis: the difference between concentration and content in iron MRI. *Hum Brain Mapp*. 2021;42(5):1463-1474. doi:10.1002/hbm.25306